Radiation Physics and Chemistry 208 (2023) 110949

Contents lists available at ScienceDirect

Radiation Physics and Chemistry

journal homepage: www.elsevier.com/locate/radphyschem

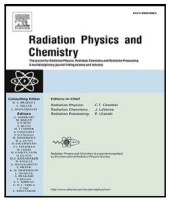

Bremsstrahlung production from 10–30 MeV electrons incident on thick targets: Monte Carlo simulation with PENELOPE

P.A. García-Higueras [a], S. García-Pareja [b], F. Salvat [c], A.M. Lallena [d,e,*]

[a] U. G. C. Radiofísica Hospitalaria, Hospital Universitario de Jaén, Avda. Ejército Español 10, E-23007 Jaén, Spain
[b] U. G. C. Radiofísica Hospitalaria, Hospital Universitario Regional de Málaga, Avda. Carlos Haya s/n, E-29010 Málaga, Spain
[c] Facultat de Física (FQA and ICC), Universitat de Barcelona, E-08028 Barcelona, Spain
[d] Departamento de Física Atómica, Molecular y Nuclear, Universidad de Granada, E-18071 Granada, Spain
[e] Instituto de Investigación Biosanitaria (ibs.GRANADA), Complejo Hospitalario Universitario de Granada/Universidad de Granada, E-18016 Granada, Spain

ARTICLE INFO

Keywords:
Bremsstrahlung production
Thick targets
Monte Carlo
PENELOPE
Optimal simulation parameters

ABSTRACT

Purpose : To study the effect of the user-defined electron/positron simulation parameters C_1 and C_2 of the Monte Carlo code PENELOPE on the results from simulations of bremsstrahlung photons generated by high energy electrons incident on thick targets.

Methods: The version 2018 of the code system PENELOPE, with four different sets of simulation parameters, is used to calculate the photon fluences produced by electron beams with initial energies ranging between 10 and 30 MeV impinging on thick elemental targets of Be, Al and Pb. Using the calculated fluences, the integrated photon yields and the mean energies of the detected photons are also evaluated. The Monte Carlo results are compared to the available experimental data, the comparison being quantified by means of χ^2 statistics.

Results: Although acceptable agreement of simulation results with experimental data is found for all the simulations performed, a significant improvement in this agreement is observed when the parameter values $C_1 = C_2 = 0.01$ or 0.001 are used, that is, when the simulations are more detailed. In the case of the mean energy of the detected photons, similar results are obtained in all the simulations. The results obtained with this version of the code improve those found with older versions in case of the Pb target.

Conclusions: Regarding the emission of bremsstrahlung photons by MeV electrons, simulations with $C_1 = C_2 = 0.01$ produce results that approximate the experimental data equally well as more detailed simulations with $C_1 = C_2 = 0.001$, with a reduction of the simulation time between 81% and 89%, depending on the initial energy of the electrons.

1. Introduction

The term bremsstrahlung designates the photon emission that occurs when fast charged particles are accelerated in the field of atoms. This emission mechanism originates the continuous background of photons in radiation beams from X-ray generators, from synchrotrons and cyclotrons, from radioactive sources with nuclides decaying through beta emission, and from galaxies and clusters.

In medical physics, bremsstrahlung emission has a crucial role as the main process for the production of photon beams in clinical electron linear accelerators, which result from the interactions of high energy electrons with a material target made of high atomic number elements. Precise characterization of these photon beams is required to account, with the prescribed accuracy, for the dose distribution in patients and for overall dosimetry studies of the photon beams themselves.

There are a few publications reporting measurements of bremsstrahlung resulting from the interaction of MeV electrons with targets of different elemental materials. In their pioneering work, Lanzl and Hanson (1951) analyzed the angular distribution of bremsstrahlung produced by 17 MeV electron beams impinging on Be, Al, Cu, Ag, and Au targets. Dance et al. (1968) measured the radiation emitted by electrons with energies of 0.5, 1.0, 2.0, and 2.8 MeV that were completely stopped in targets of Al and Fe. Rester et al. (1970) extended the work of Dance et al. by performing measurements for electron beams of 0.2, 1.0, and 2.0 MeV incident on Sn, Au and Be targets, 2.8 MeV beams on Sn and Au, and 0.2 MeV beams on Al and Fe. Nakamura and Hirayama (1976) studied the emission from thick lead targets bombarded by electrons with energies between 15 and 25 MeV. More recently, Faddegon et al. (1990, 1991) studied the bremsstrahlung

* Corresponding author.
E-mail addresses: pantonio.garcia.sspa@juntadeandalucia.es (P.A. García-Higueras), salvador.garcia.sspa@juntadeandalucia.es (S. García-Pareja), cesc@fqa.ub.edu (F. Salvat), lallena@ugr.es (A.M. Lallena).

https://doi.org/10.1016/j.radphyschem.2023.110949
Received 7 February 2023; Received in revised form 6 March 2023; Accepted 28 March 2023
Available online 30 March 2023

radiation produced by electron beams of 10, 15, 20, 25, and 30 MeV on thick Al and Pb targets, and of 15 MeV electrons on Be targets.

Nowadays, Monte Carlo simulation of clinical accelerators has became a usual tool as a component either of treatment planning systems or of complementary verification procedures (Brualla et al., 2017). However, the simulation of bremsstrahlung is far from trivial because of the complexity of the associated differential cross section (DCS), with strong correlations between the energy and the direction of emission of the released photon, and because photon emission may occur at any stage along an electron history. This difficulty has motivated many benchmark comparisons of results from various available Monte Carlo codes with measurements. Thus, Sempau et al. (2003) and Salvat et al. (2006) found generally good agreement between measured bremsstrahlung energy spectra and results from the PENELOPE code for electrons with energies up to 1 GeV impinging on Al, Au, Pb and water targets. Faddegon et al. (2008) performed a general study of results from the codes EGSnrc, Geant4 and PENELOPE. They analyzed different magnitudes such as the bremsstrahlung yield, the angular and energy distributions of photon fluences, etc., and concluded that EGSnrc and PENELOPE gave results closer to measurements, though the three codes overestimated the photon spectra at low energies. Finally, Pandola et al. (2015) have found overall good agreement between their Geant4 simulations and the experimental data of Dance et al. (1968) and Rester et al. (1970). The influence of the PENELOPE simulation parameters on the accuracy of the Monte Carlo results was also investigated, in the context of X-ray spectroscopy, by Llovet and Salvat (2018).

In a simulation study using the PENELOPE code, Rodriguez et al. (2015) have drawn attention about the values of the simulation parameters to be considered in the target of a Varian Clinac 2100 operated at 6 MV to ensure agreement of simulation results with measurements. They concluded that, to avoid significant deviations of the dose in the phantom or the patient, the parameters C_1 and C_2, which are the ones determining the accuracy of the simulation, should have values less than 0.001. This conclusion is at variance with the safe values $C_1 = C_2 = 0.05$ recommended in the PENELOPE manual (Salvat, 2020), and used by Sempau et al. (2003) and Faddegon et al. (2008). The observation of Rodriguez et al. (2015) indicates that the emission of high-energy bremsstrahlung photons from thick targets is very sensitive to the accuracy with which the first stages of the electron trajectories in the target are simulated, because it is at these first stages where high-energy photons are released. The large distance from the target to the photon detector, or to the patient's body, acts as a kind of magnifying lens in revealing inconsistencies in the energy-angle distribution of bremsstrahlung photons. Hence, it is important to analyze the dependence of the simulated distributions on the adopted values of the parameters C_1 and C_2. It is worth mentioning here that the description of the intrinsic angular distribution of bremsstrahlung photons has been improved in the 2018 version of the code by largely increasing the size of the calculated shape-function database (for details, see Salvat, 2020).

The present work aims at analyzing the influence of the parameters C_1 and C_2 on the reliability of simulated bremsstrahlung emission, and to devise accurate schemes to simulate the emission from thick targets. For this purpose, we performed a series of simulations using the last available version of PENELOPE (Salvat, 2020), with the geometrical arrangements of experiments described in detail, and we compared the simulation results with measured data from the experiments by Faddegon et al. (1990, 1991).

2. Material and methods

2.1. Tracking parameters in PENELOPE

PENELOPE simulates the coupled transport of electrons, positrons and photons with energies from, nominally, 50 eV up to 1 GeV in geometries consisting of homogeneous bodies of arbitrary composition limited by quadric surfaces. Photons are simulated in a detailed way, that is, interaction by interaction, while electrons and positrons are simulated through an elaborate mixed scheme. The code classifies the interaction events of these charged particles as hard and soft, by means of a cutoff angular deflection θ_c for elastic collisions, and cutoff energy transfers W_{cc} and W_{cr} for inelastic collisions and bremsstrahlung emission, respectively. Hard events are those involving angular deflections (in elastic collisions) or energy transfers larger than the corresponding cutoffs; they are simulated in detail from the corresponding restricted DCSs. The aggregate effect of the soft events (*i.e.*, events involving sub-cutoff energy transfers or elastic angular deflections) that occur between each pair of consecutive hard events are simulated as a single artificial event (a hinge) by using a multiple scattering approach.

The mixed simulation of electrons and positrons is tuned by means of the following user-defined simulation parameters (Salvat, 2020):

- C_1, which sets an upper limit to the average angular deflection $\overline{\theta}_{ms}$ due to the multiple scattering events occurring in a trajectory step between successive hard elastic collisions: $C_1 \simeq 1 - \cos\overline{\theta}_{ms}$;
- C_2, which limits the average fractional energy loss, $C_2 = \overline{\Delta E}_{el}/E_{el}$, of a particle with kinetic energy E_{el} along a trajectory step between successive hard elastic collisions;
- W_{cc}, which fixes the cutoff energy loss separating soft and hard inelastic collisions;
- W_{cr}, which establishes the cutoff energy loss separating soft and hard bremsstrahlung emission events, and
- s_{max}, which sets the maximum step length.

In the present work, simulations of bremsstrahlung emission from thick targets have been performed. In this kind of simulations, the value of s_{max}, which allows a minimum number of steps in thin bodies, ensuring the reliability of the results, is irrelevant and it has been set to 10^{20}. The parameters, W_{cc} and W_{cr} are expected to have practically no effect; they have been chosen to be 200 keV and 10 keV, respectively, for all the materials present in the simulated arrangement. These are the same values used in the work by Faddegon et al. (2008).

For the purposes of the present work, the only parameters that effectively affect the accuracy of simulation results are C_1 and C_2, which determine the value of the mean free path between hard elastic collisions and the corresponding cutoff angular deflection θ_c. As shown in the manual of PENELOPE (Salvat, 2020), each of these parameters is effective for particles with energies in different ranges: C_2 only for very high kinetic energies (above ~10 MeV), and C_1 for intermediate energies (between ~10 keV and ~10 MeV). When the kinetic energy of the transported particle becomes lower than a certain value (determined by the program), the simulation of elastic collisions is gradually switched to detailed mode. The lower the values of C_1 and C_2, the more accurate are the simulation results, at the expense of longer calculation times. The numerical values of these two parameters can be chosen independently within the range [0.0–0.2]. However, as their effects do not interfere, they are usually given the same value. The PENELOPE manual (Salvat, 2020) suggests that the value $C_1 = C_2 = 0.05$ is "safe", in the sense that simulation results are sufficiently accurate for most practical purposes.

In this work, four sets of simulations were performed with the values of $C_1 = C_2 = C$ equal to 0.2, 0.1, 0.01 and 0.001, which correspond to increasingly more accurate, and slower, simulations.

In all the simulations reported here, the absorption energies for electrons and positrons were set to 200 keV, and that of photons to 10 keV for all materials in the simulation geometry; these values were also adopted in Faddegon et al. (2008).

2.2. Description of the reported simulations

Our analysis is based on measured data from the experiments by Faddegon et al. (1990, 1991). Table 1 summarizes the energies of the electron beams, E_e, and the thicknesses of the target materials, t, used in the experiments and adopted in our simulations. The

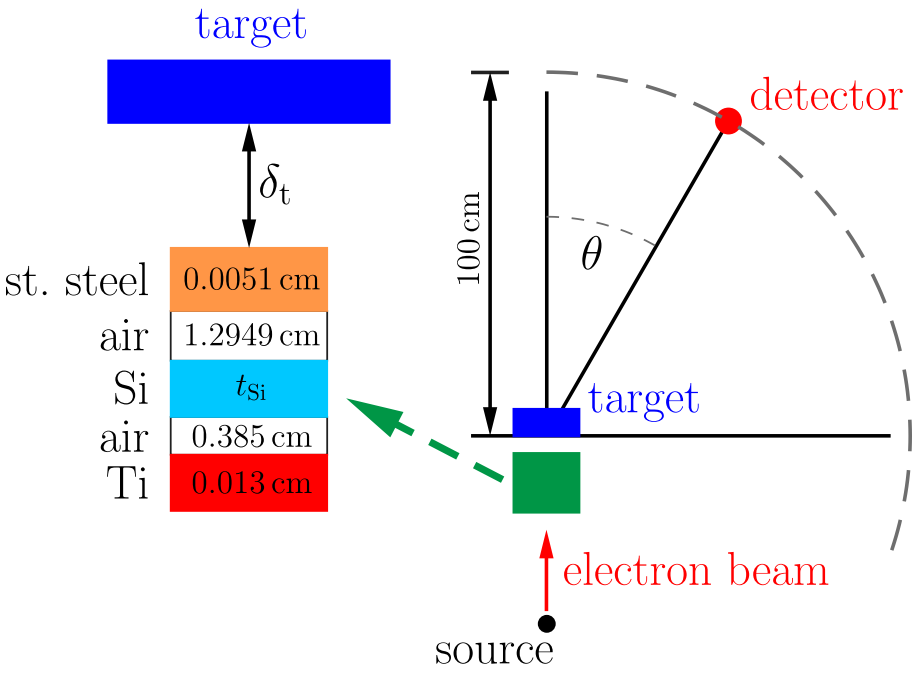

Fig. 1. Scheme (not to scale) of the geometry used in the simulations performed in the present work. The composite structure, sketched in the left diagram, consists of various material slabs, whose compositions and thicknesses are indicated. The distance δ_t from that structure to the target is 0.94 cm for Al and Be targets and 1.6 cm for Pb targets. The thickness of the Si slab is $t_{Si} = 0.01$ cm for the 15 MeV electron beams and 0.015 cm for the other beam energies.

Table 1
Electron beam energies, E_e (nominal values and values used in the simulations), and thicknesses, t, of the various targets used in the experiments of Faddegon et al. (1990, 1991) and considered in the present simulations.

E_e [MeV]		t [g cm^{-2}]		
Nominal	Simulation	Be	Al	Pb
10.0	10.09		6.480	6.800
15.0	15.18	11.670	9.740	9.130
20.0	20.28		11.620	11.340
25.0	25.38		15.130	11.340
30.0	30.45		16.210	13.610

electron beam energies considered in the present simulations (second column of Table 1) are those used by Faddegon et al. (2008) in their simulations; these values were obtained by those authors after an accurate re-calibration of the setup used in the benchmark experiments by Faddegon et al. (1990, 1991). The target thicknesses are about 1.1 times the electron range, calculated from the continuous slowing down approximation, for the corresponding electron beam energies. For the 10, 20, 25, and 30 MeV electron beams, only data measured at $\theta = 0^o$ are available. For the 15 MeV electron beam, photons were detected at $\theta = 0^o$, 1^o, 2^o, 4^o, 10^o, 30^o, 60^o, and 90^o.

Fig. 1 shows a scheme of the geometry employed in the simulations. As the data of Faddegon et al. were corrected for the effects due to the transport in air and the detector (Faddegon et al., 1990, 1991), the whole experimental arrangement is assumed to be in vacuum. In the simulations, an electron beam of square transverse section with a side length of 0.35 cm impinged normally on the lower surface of a composite structure consisting of various material slabs of the indicated compositions and thicknesses. This structure represents the Ti window at the exit of the accelerating stage, a transmission current monitor of Si, and an evacuated ionization chamber with an entrance window of stainless steel. The ionization chamber was employed only for small angle measurements; it was removed and replaced by air for measurements at angles between 30^o and 90^o. After crossing that structure, electrons reach the target, which is at a distance δ_t above the upper surface of the structure. A photon detector placed at 1 m from the target was used to record the photon energy spectra. The laboratory frame of coordinates used in the simulations had its origin at the center of the irradiated surface of the target with its Z axis coinciding with the symmetry axis of the setup.

The relevant simulation results were the energy distributions of photons reaching an annular detector at a distance $d = 1$ m from the origin of coordinates covering the interval of polar angles $(\theta - \delta, \theta + \delta)$ with $\delta = 0.5^o$. The detector at $\theta = 0^o$ covered the polar-angle interval $(0^o, 0.5^o)$.

The simulation code calculated the bremsstrahlung yield

$$\frac{\mathrm{d}S}{\mathrm{d}E} = \frac{1}{N_e} \frac{\mathrm{d}^2 N_\gamma}{\mathrm{d}E\, \mathrm{d}\Omega}, \tag{1}$$

where $\mathrm{d}^2 N_\gamma/(\mathrm{d}E\, \mathrm{d}\Omega)$ is the number of photons that reach a detector per unit energy and per unit solid angle [in units of (MeV·sr)$^{-1}$] and N_e is the number of simulated primary electron histories. In order to be consistent with Faddegon et al. (2008) the output bremsstrahlung yields were converted into photon energy fluences f, defined as

$$f = E \frac{\mathrm{d}S}{\mathrm{d}E} \frac{1}{d^2}, \tag{2}$$

and given in units of m^{-2}. The photon energy E is introduced to reduce the variation range of the quantity, and to produce cleaner plots.

To quantify the comparison of simulation results with experimental data, it is necessary to consider their associated uncertainties. The overall uncertainty in the measurements (Faddegon et al., 1990, 1991) varies between 3.7% at the beam axis and 2.3% for directions at angles with the beam axis of 4^o or larger. The statistical uncertainties of simulation results are determined by the number of generated random electron histories in each simulation run. The number of generated showers induced by primary electrons varied between $3 \cdot 10^7$, for $E_e = 30$ MeV, and $3 \cdot 10^8$, for $E_e = 10$ MeV. The relative statistical uncertainties of the simulated results are less than about 2% at the maxima of the photon energy-fluence curves.

2.3. Benchmark comparisons of the Monte Carlo results

The consistency of the Monte Carlo simulations was analyzed by using the χ^2 statistics to compare the photon energy fluences obtained with various values of the simulation parameter C ($= C_1 = C_2$). For each electron energy, target, and photon detection angle, the Monte Carlo simulation with a given C value gave a set of photon energy fluence data and their associated statistical uncertainties, $\{[f_k^{\mathrm{MC}}(C), \sigma_k^{\mathrm{MC}}(C)], k = 1, 2, \ldots, M\}$, where the index k runs over the bins of the simulated photon energy spectrum (a histogram). We performed simulations with $C = 0.2$, 0.1, 0.01, and 0.001. Because, in principle, PENELOPE simulations are more accurate the smaller the value of C (Salvat, 2020), we consider the results for $C = 0.001$ as the reference. To analyze the convergence of the Monte Carlo results as C decreases, we calculate the quantity

$$\chi^2_{\mathrm{MC}}(C) = \frac{1}{M}\sum_{k=1}^{M}\left[\frac{f_k^{\mathrm{MC}}(C) - f_k^{\mathrm{MC}}(C=0.001)}{\sigma_k^{\mathrm{MC}}(C=0.001)}\right]^2, \quad C = 0.2,\ 0.1,\ 0.01\,. \tag{3}$$

The comparison between simulation results and the experimental data of Faddegon et al. (1990, 1991) was quantified in a similar way. For given electron energy, target and photon detection angle, we have a set of measured values of the photon energy fluence: $\{(f_k^{\mathrm{exp}}, \sigma_k^{\mathrm{exp}}), k = 1, 2, \ldots, N\}$. Because the binning used in the simulations does not always match the experimental energy grid, the values of the Monte Carlo energy fluences at the points of the experimental energy grid, $\{(f_k^{\mathrm{MC}}, \sigma_k^{\mathrm{MC}}), k = 1, 2, \ldots, N\}$, were calculated by linearly interpolating the original Monte Carlo data. To quantify the comparison, we used the reduced χ^2 value, defined as:

$$\chi^2_{\mathrm{exp}}(C) = \frac{1}{N}\sum_{k=1}^{N}\left[\frac{f_k^{\mathrm{MC}}(C) - f_k^{\mathrm{exp}}}{\sigma_k^{\mathrm{exp}}}\right]^2, \quad C = 0.2,\ 0.1,\ 0.01,\ 0.001\,. \tag{4}$$

In order to reveal anomalously large local differences, we also considered the normalized partial χ^2,

$$\chi^2_{\mathrm{partial}}(C) = \frac{1}{N}\sum_{k=1}^{n}\left[\frac{f_k^{\mathrm{MC}}(C) - f_k^{\mathrm{exp}}}{\sigma_k^{\mathrm{exp}}}\right]^2, \quad C = 0.2,\ 0.1,\ 0.01,\ 0.001\,, \tag{5}$$

obtained by restricting the sum in Eq. (4) to the first n data.

In addition, the uncertainties of χ^2_{MC} and χ^2_{exp}, which result from the statistical uncertainties of the Monte Carlo data, were estimated as follows. A number of pseudo-fluences (usually 10^3) were generated by random sampling from the normal distribution $\mathrm{N}[f_k^{\mathrm{MC}}(C), \sigma_k^{\mathrm{MC}}(C)]$ of each simulated fluence datum, the corresponding χ^2 values were obtained by comparing these pseudo-fluences with either the Monte Carlo fluences for $C = 0.001$ or the experimental data. The uncertainty of χ^2_{MC} or χ^2_{exp} was estimated from the distribution of the values so obtained.

2.4. Photon yields and average photon energies

Using the experimental and Monte Carlo energy fluences, we calculated the photon yield, *i.e.* the average number of photons that enter the detector per primary electron,

$$\mathcal{Y}(\theta) = \Delta\Omega \int_{E_{\mathrm{min}}}^{E_{\mathrm{max}}} \frac{\mathrm{d}S}{\mathrm{d}E}\,\mathrm{d}E \tag{6}$$

and the average energy of the detected photons,

$$\overline{E}_\gamma(\theta)) = \frac{1}{\mathcal{Y}(\theta)}\,\Delta\Omega \int_{E_{\mathrm{min}}}^{E_{\mathrm{max}}} E\,\frac{\mathrm{d}S}{\mathrm{d}E}\,\mathrm{d}E\,, \tag{7}$$

where $\Delta\Omega$ is the solid angle covered by the detector. For consistency with the measured data, the lower limit of the integrals was $E_{\mathrm{min}} = 0.145$ MeV for the 15 MeV electron beam, and $E_{\mathrm{min}} = 0.220$ MeV for the other beams. The energy E_{max} is the highest energy of the detected photons in each case. The uncertainties of $\mathcal{Y}(\theta)$ and $\overline{E}_\gamma(\theta))$ were obtained from a Monte Carlo sampling method, similar to the one described in the previous section, that is, using pseudo-fluences obtained by random sampling from normal distributions.

The comparison between the corresponding simulation results and experimental data has been carried out by considering χ^2 statistics defined similarly to those of the fluences.

Table 2
Average χ^2_{MC} values obtained by considering all data involved in the analysis, all data corresponding to each of the three targets studied, all data for the 15 MeV electron beam, and all data corresponding to a detection angle of 0°. The last column indicates the number of data considered in each case. Other average values involving less than 4 data are not shown.

	$C = 0.2$	$C = 0.1$	$C = 0.01$	# data
all	17.0(0.7)	12.5(0.6)	2.2(0.3)	32
Be	24.8(0.9)	18.0(0.7)	2.3(0.3)	8
Al	17.2(0.8)	13.6(0.7)	2.2(0.3)	12
Pb	11.6(0.6)	7.9(0.5)	2.2(0.3)	12
15 MeV	17.8(0.7)	12.5(0.6)	2.2(0.3)	24
0°	13.5(7)	11.8(0.7)	2.3(0.3)	11

3. Results and discussion

3.1. Simulated photon energy fluences

Fig. 2 shows the comparison between various photon energy fluences obtained from our simulations. In particular, those for $C = 0.2$ (red solid curves) and 0.01 (blue dashed curves) are compared to the fluences obtained from our most detailed simulations with $C = 0.001$ (black solid symbols). In the first three panels, the fluences corresponding to the 15 MeV electron beam and photon detection angles of 1^0, 4^0, 10^0, 30^0, 60^0, and 90^0 are shown for the Be (Fig. 2a), Al (Fig. 2b), and Pb (Fig. 2c) targets; in the two rightmost panels, the fluences for a photon detection angle of 0^0 and for electron beam energies of 10, 15, 20 and 30 MeV are shown for Al (Fig. 2d) and Pb (Fig. 2e) targets.

Differences between the simulated fluences are larger the lighter the target and the smaller the detection angle. This can be seen quantitatively in Fig. 3, where the $\chi^2_{\mathrm{MC}}(C)$ values, defined in Eq. (3), are shown. The general trend is that χ^2_{MC} reduces as C decreases. The values found for $C = 0.01$ are smaller than 3, the only exception being that of the 10 MeV beam in Al at 0^o where $\chi^2_{\mathrm{MC}}(C = 0.01) = 3.8$ (red squares in Fig. 3b). Only in three cases (Be, 15 MeV, 60^o and 90^o, and Pb, 15 MeV, 90^o), the value of $\chi^2_{\mathrm{MC}}(C = 0.01)$ is larger than $\chi^2_{\mathrm{MC}}(C = 0.2)$. It must be also indicated that the largest relative uncertainties of χ^2_{MC} were found in the case of Be, for the 15 MeV electron beam and a photon detection angle of 90^o: 24% for $C = 0.2$, 22% for $C = 0.1$, and 19% for $C = 0.01$.

It is worth noting that the average χ^2_{MC} values shown in Table 2 confirm this general behavior. The results obtained for $C = 0.01$ are, in general, closer to those corresponding to the more detailed simulations with $C = 0.001$, than the fluences obtained for the larger C values. The average χ^2_{MC} changes from values well above 10 for $C = 0.2$ and 0.1 to ~ 2 for $C = 0.01$, indicating that the results converge when C is decreased.

3.2. Comparison with the experimental photon energy fluences

Fig. 4 shows the comparison between the photon energy fluences obtained in two of our simulations, those for $C = 0.2$ (red solid curves) and $C = 0.01$ (blue dashed curves), with the experimental data of Faddegon et al. (1990, 1991). In the first three panels, the fluences for an electron beam of 15 MeV and photon detection angles of 1^0, 4^0, 10^0, 30^0, 60^0, and 90^0 are shown for the Be (Fig. 4a), Al (Fig. 4b), and Pb (Fig. 4c) targets; in the last two panels, the fluences in the beam direction (with the photon detection angle of 0^0), for electron beam

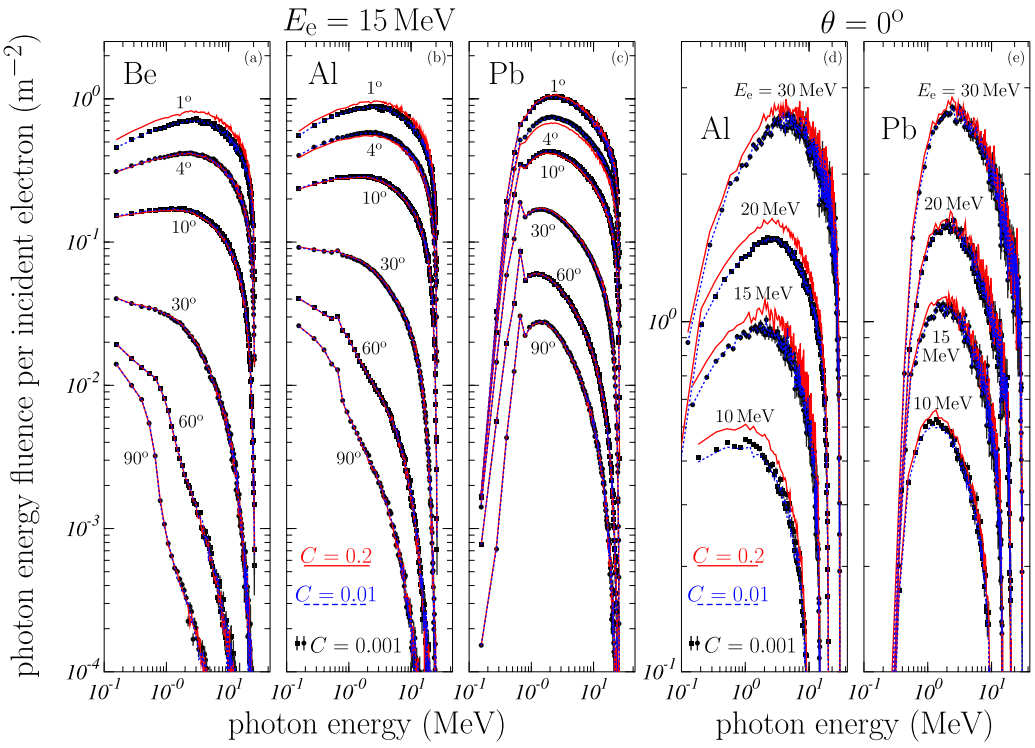

Fig. 2. Simulated photon energy fluences for the 15 MeV electron beam, in (a) Be, (b) Al and (c) Pb targets and various photon detection angles, and for the electron beams of 10, 15, 20 and 30 MeV, in (d) Al, and (e) Pb targets and for a photon detection angle of 0°. Fluences obtained for $C = 0.2$ (red solid curves) and $C = 0.01$ (blue dashed curves) are compared to those found for $C = 0.001$ (black solid symbols). The relative uncertainties of the various fluences are of similar magnitude; only those for $C = 0.001$ are displayed.

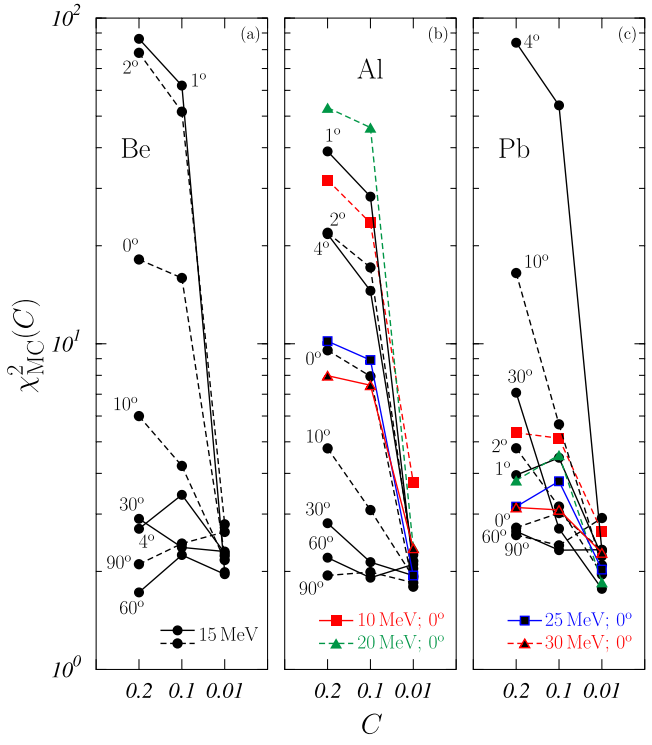

Fig. 3. χ^2_{MC} values, as defined by Eq. (3), obtained for (a) Be, (b) Al, and (c) Pb targets. The values of the detection angles are indicated in the case of the 15 MeV electron beam (black open and solid circles); for the other electron beam energies (10, 20, 25 and 30 MeV) the detection angle is 0°. Uncertainties are not shown for clarity of the figure (see text).

energies of 10, 15, 20 and 30 MeV are shown for Al (Fig. 4d) and Pb (Fig. 4e) targets.

Generally, good agreement between simulation results and experimental data is found for photon energies above a few MeV. The only exceptions correspond to Be target, for the 15 MeV beam and photon detection angles of 60° and 90°. Therein the Monte Carlo fluences underestimate the experimental data. This result was also pointed out by Faddegon et al. who benchmarked several Monte Carlo codes against these data. In this respect, they indicated that measurements could be erroneous in these two cases due to the low counting statistics in that region and to high-energy electron contamination in the detector (Faddegon et al., 2008). At low energies some discrepancies appear that are larger for $C = 0.2$ (red solid curves) than for $C = 0.01$ (blue dashed curves).

These features can be seen quantitatively in Fig. 5 that shows all the χ^2_{exp}, as defined by Eq. (4), found in the comparison between the Monte Carlo results and the experimental fluences. In contrast to what has been seen in Fig. 3, here an overall trend is not observed. In fact we see two different situations. One corresponds to values of χ^2_{exp} that are almost independent of C. This occurs in 13 cases, all of them for 15 MeV beams, and for detection angles of 4° or larger in Be and Al and 30°, 60°, and 90° in Pb. The second situation is similar to that observed for the comparison between the Monte Carlo fluences: the χ^2_{exp} obtained for $C = 0.01$ and $C = 0.001$ are clearly smaller than those obtained for the other two highest C values. However in 13 cases out of the remaining 19, an unexpected result is found: $\chi^2_{exp}(C = 0.01) < \chi^2_{exp}(C = 0.001)$. The opposite is true for 15 MeV, 2° in Be and Al, 20 MeV, 0° in Al and Pb, 25 MeV, 0° in Al, and 30 MeV, 0° in Pb. In what refers to the relative uncertainties, the largest values are found in the case of Pb, for an electron beam of 15 MeV and a photon detection angle of 0°: 16% for $C = 0.2$, 17% for $C = 0.1$, 26% for $C = 0.01$, and 20% for $C = 0.001$. These values are similar to those found for the comparison between Monte Carlo fluences.

In Table 3 we quote the corresponding averages obtained when the χ^2_{exp} values are grouped in different ways. It is worth noting that

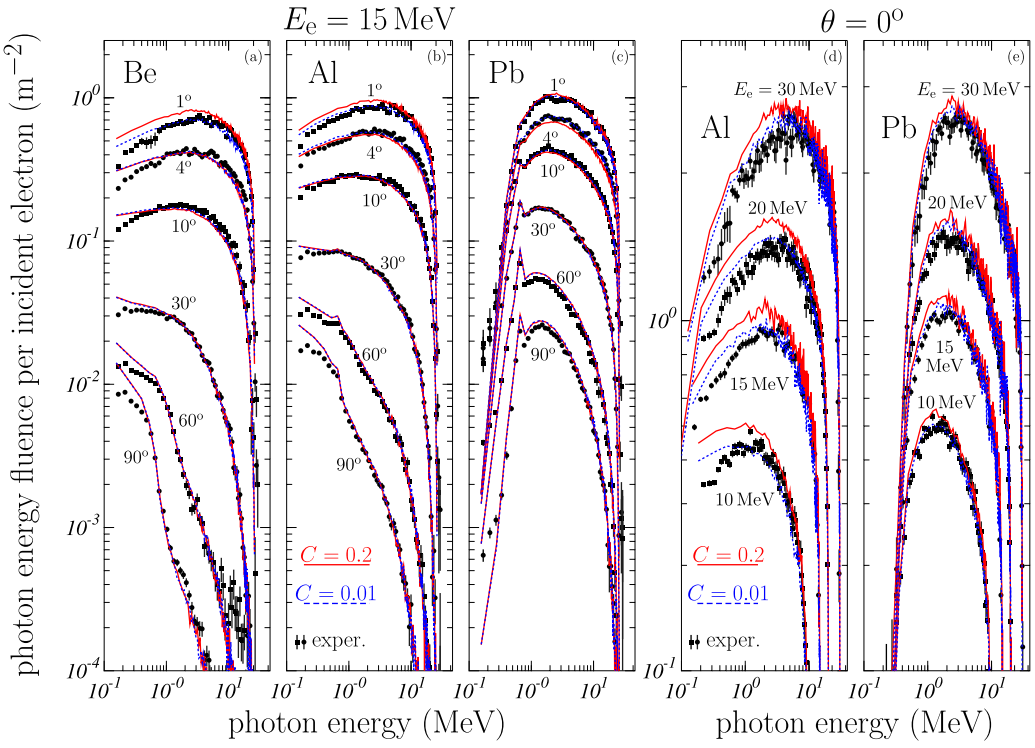

Fig. 4. Photon energy fluences for the 15 MeV electron beam, for (a) Be, (b) Al and (c) Pb targets and various photon detection angles, and for the electron beams of 10, 15, 20 and 30 MeV, for (d) Al, and (e) Pb targets and for a photon detection angle of 0°. Fluences obtained for $C = 0.2$ (red solid curves) and $C = 0.01$ (blue dashed curves) are compared to the experimental data (black solid symbols). Uncertainties of the calculated fluences are not shown for clarity of the figure.

Table 3
Average χ^2_{exp} values found for all data considered in the analysis, for all data corresponding to each of the three targets studied, for all data obtained for the 15 MeV electron beam and for all data corresponding to a detection angle of 0°. The last column indicates the number of data considered in each case. Other average values involving less than 4 data are not shown.

	$C = 0.2$	$C = 0.1$	$C = 0.01$	$C = 0.001$	# data
all	31.8(1.4)	31.1(1.5)	24.5(1.2)	25.2(1.2)	32
Be	73.6(2.5)	73.9(2.5)	61.5(2.2)	63.1(2.2)	8
Al	25.8(0.8)	24.1(0.8)	17.3(0.6)	17.6(0.7)	12
Pb	9.9(0.8)	9.7(0.9)	7.2(0.6)	7.7(0.7)	12
15 MeV	37.8(1.6)	37.4(1.6)	31.2(1.4)	32.1(1.4)	24
0°	21.1(1.3)	19.2(1.3)	6.2(0.8)	6.7(0.8)	11

the values obtained for $C = 0.2$ and $C = 0.1$ coincide within the associated statistical uncertainties. However, the results for $C = 0.01$ imply a significant reduction of the average χ^2_{exp} (21% when all data are included, 17% for Be, 28% for Al, 26% for Pb, 17% for the 15 MeV data, and 68% for the 0° data.) In all the cases included in Table 3 the average χ^2_{exp} obtained with $C = 0.001$ is slightly larger than those for $C = 0.01$ (though statistically compatible if uncertainties are taken into account).

It is interesting to come back to the results of Be for large photon detection angles. As said above, there are some doubts about the high energy measurements for the Be target and photon detection angles of 60° and 90°. As seen in Fig. 5, these two cases give the largest values of χ^2_{exp}. In order to explore the source of these large χ^2 values, we show in Fig. 6 the quantity $\chi^2_{partial}/\chi^2_{exp}$ as a function of the energy of the detected photons (normalized to its maximum value). Results for Be, for the electron beam of 15 MeV and for detection angles of 30°, 60°, and 90° are shown. We have included here the ratios obtained for $C = 0.001$, but similar results are found for the other C values analyzed.

The important aspect to be noted is that 60% at least of the total χ^2_{exp} is due to the first data, those with the lower energies. The contributions of the data at high photon detection energies are relatively small, despite what has been commented above regarding the discrepancies observed in the high energy tails of the measured fluences (cf. Fig. 4).

As mentioned in the Introduction, the version 2018 of PENELOPE improved the description of the angular distribution of the bremsstrahlung photons. Originally, the code used a parameterization of the angular shape function with coefficients obtained by interpolation of a limited sample with 144 shape functions calculated by the partial-wave method. The 2018 version of the code uses a larger database with 910 partial-wave shape functions covering the relevant intervals of atomic number, projectile energy, and photon energy uniformly, which effectively removes the interpolation uncertainties of the original sparse grid. Results obtained in the present work (with the 2018 version) are compared with those from the 2014 version (which was used in the calculations of Faddegon et al., 2008) in Fig. 7.

The results for Al (red circles) indicate there is practically no difference between the two versions of the code because the χ^2 ratio is close to 1. The situation is quite different for Pb (green squares), for which the ratio takes values generally less than unity, indicating that the new version describes the experimental data better. Interestingly, Al was included in the original database of shape distributions, but not Pb. Our results thus confirm that the extended database does improve the accuracy of the angular distributions used in the simulation.

To complete the discussion, it is worthwhile to analyze the savings in computational time resulting from using $C = 0.01$ instead of $C = 0.001$, as both alternatives produce results that are similarly accurate. Table 4 shows the simulation speeds, in showers per second, corresponding to the simulations with $C = 0.01$ and $C = 0.001$. The last column in the Table is the value

$$\delta = \frac{v(C = 0.01) - v(C = 0.001)}{v(C = 0.01)}, \tag{8}$$

where v are the simulation speeds. The quantity δ measures the reduction in CPU time obtained by running the simulations with $C = 0.01$ instead of $C = 0.001$.

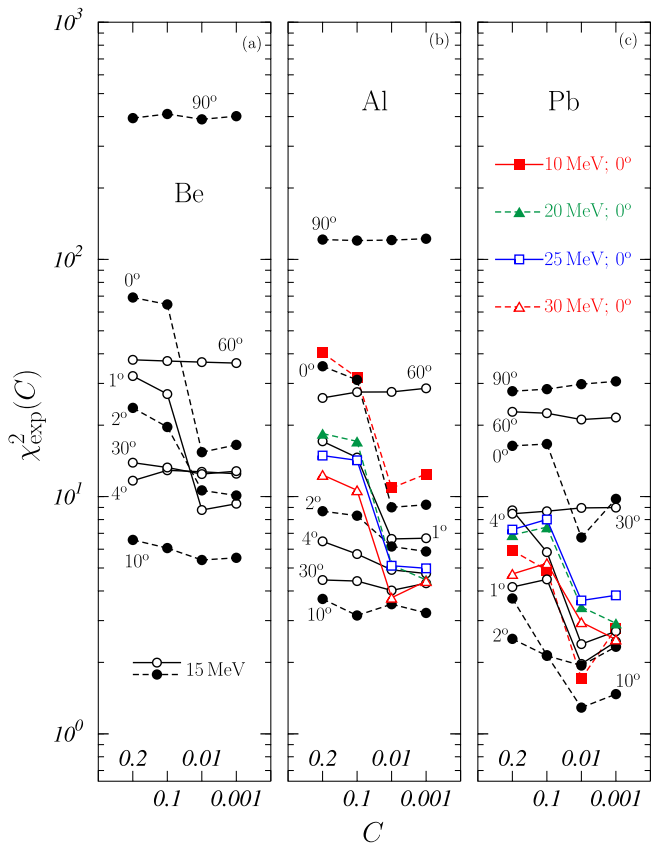

Fig. 5. χ^2_{exp} values, as defined in Eq. (4), obtained for (a) Be, (b) Al, and (c) Pb. The values of the detection angles are indicated in the case of the 15 MeV electron beam (black open and solid circles); for the other electron beam energies (10, 20, 25 and 30 MeV) the detection angle is 0°. Uncertainties are not shown for clarity of the figure (see text).

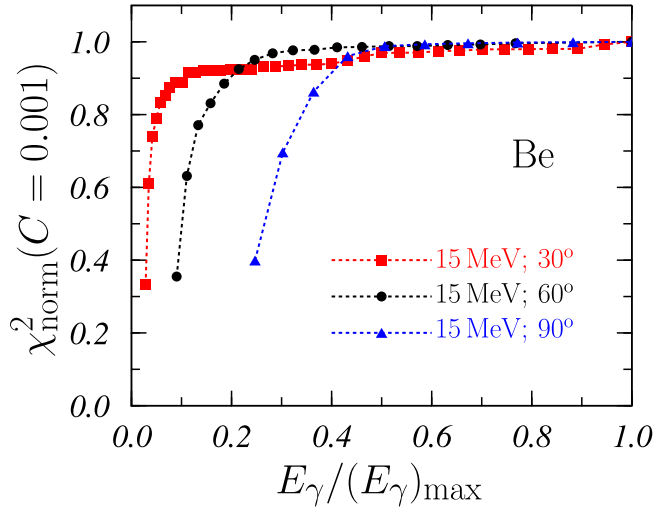

Fig. 6. Normalized $\chi^2_{norm} = \chi^2_{partial}(C)/\chi^2_{exp}$ values obtained for $C = 0.001$, the Be target, an electron beam energy of 15 MeV and detection angles of 30° (red squares), 60° (black circles) and 90° (blue triangles) are shown as a function of the energy of the detected photons, E_γ (normalized to the respective maximum energies $(E_\gamma)_{max}$).

For a given target, increasing the electron energy reduces the simulation speed but the CPU time reduction is roughly maintained. Also, the simulation speed reduces when the atomic number of the target increases. The CPU time reduction δ is slightly smaller in Pb.

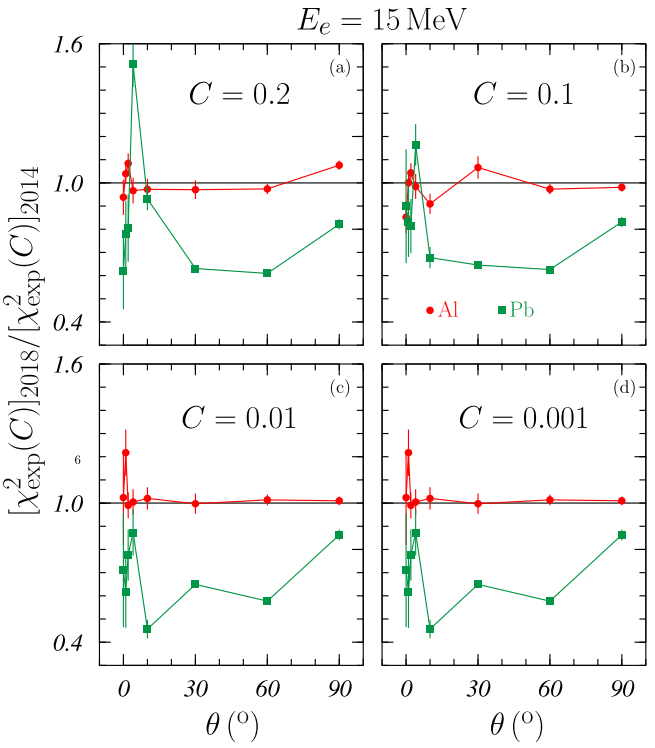

Fig. 7. Ratio of the χ^2_{exp} obtained with the versions 2018 and 2014 of PENELOPE for Al (red circles) and Pb (green squares) targets, as a function of θ, for $E_e = 15$ MeV. The results for the four values of C analyzed in this work are shown.

Table 4
Simulation speeds, in showers per second, for the simulations with $C = 0.01$ and $C = 0.001$ for various targets and initial electron energies. The last column shows the quantity δ as defined by Eq. (8).

Target		Simulation velocity [showers s^{-1}]		
	E_e (MeV)	$C = 0.01$	$C = 0.001$	δ (%)
Be	15.0	1044.0	135.6	87.0
Al	10.0	788.3	89.8	88,6
	15.0	606.2	71.9	88.1
	20.0	512.8	59.5	88.4
	25.0	446.3	49.9	88.8
	30.0	400.8	46.3	88.5
Pb	10.0	122.5	20.1	83,6
	15.0	78.5	14.6	81.4
	20.0	66.0	10.8	83.6
	25.0	56.1	9.5	83.1
	30.0	46.5	8.0	82.8

3.3. Photon yields and mean photon energies

Fig. 8 compares experimental and Monte Carlo photon yields, Eq. (6), and mean energies of detected bremsstrahlung photons, Eq. (7). The experimental data quoted in Faddegon et al. (1990, 1991) are represented with black solid triangles, whereas the Monte Carlo results obtained with $C = 0.2$, $C = 0.1$, $C = 0.01$, and $C = 0.001$ are indicated with red open squares, green solid circles, blue solid squares and black open circles, respectively.

In general, the description of the photon yield and the average energy of detected photons is fairly realistic, independently of the value of C chosen for the Monte Carlo simulations. In the case of the photon yields, panels (a)–(e), the Monte Carlo results obtained with the lower C values are closer to the experimental yields than those found with $C = 0.2$ and $C = 0.1$ that are almost overlapping in panels 8d and 8e. This situation is confirmed by the reduced χ^2 values obtained by comparing the experimental and the Monte Carlo photon yields, which

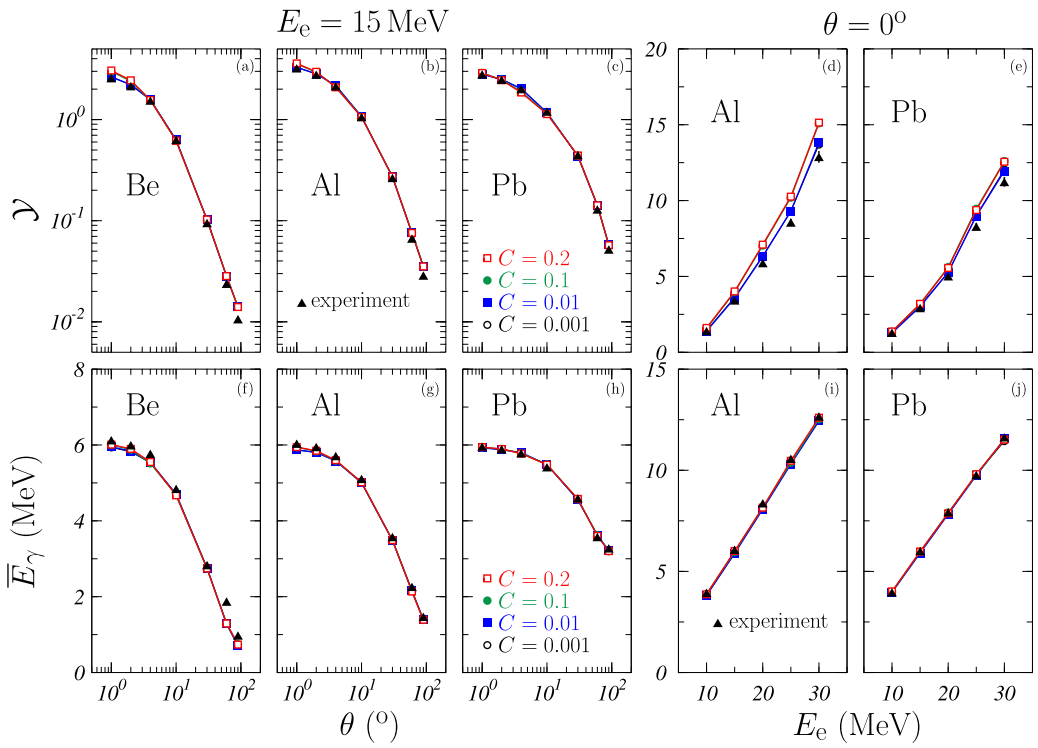

Fig. 8. Photon yields (upper panels), Eq. (6), and mean photon energies (lower panels), Eq. (7), as functions of the detection angle for the electron beam of 15 MeV (panels (a)–(c) and (f)–(h)), and as a functions of the electron beam energy for a detection angle of 0° (panels (d), (e), (i) and (j)). Monte Carlo results obtained from the present simulations with $C = 0.2$ (red open squares), $C = 0.1$ (green solid circles), $C = 0.01$ (blue solid squares) and $C = 0.001$ (black open circles) are compared to the experimental data given in Faddegon et al. (1990, 1991) (blak solid triangles).

Table 5
Reduced χ^2 values obtained from the comparison of experimental photon yields, as quoted in Faddegon et al. (1990, 1991), with those obtained from our Monte Carlo simulations with the four sets of tracking parameters. The lines in the Table are the results for all the data considered in the analysis, for all data corresponding to each of the three targets studied, for the 24 data obtained for the 15 MeV electron beam, and for all data corresponding to a detection angle of 0°, respectively. The last column indicates the number of data considered in each line. Other average values involving less than 4 data are not shown.

	$C = 0.2$	$C = 0.1$	$C = 0.01$	$C = 0.001$	# data
all	10.7(0.1)	9.9(0.1)	3.2(0.1)	3.3(0.1)	32
Be	10.6(0.1)	9.5(0.1)	4.6(0.1)	4.7(0.1)	8
Al	15.8(0.2)	14.3(0.2)	3.5(0.1)	3.6(0.1)	12
Pb	5.5(0.1)	5.8(0.2)	1.9(0.1)	2.1(0.1)	12
15.0	5.8(0.1)	5.2(0.1)	2.7(0.0)	2.8(0.1)	24
0°	22.5(0.3)	21.0(0.3)	3.6(0.1)	3.9(0.1)	11

are given in Table 5. The values of χ^2 for $C = 0.2$ and 0.1 are relatively large, while the values for both $C = 0.01$ and $C = 0.001$ are similar and much smaller.

It is worth mentioning that, for both $C = 0.01$ and $C = 0.001$, the relative differences between Monte Carlo and experimental photon yields are below 10% in all cases except for the 15 MeV electron beam and photon detection angles θ of 60° and 90° (the angles affected by the experimental difficulties mentioned above in the case of Be). In fact, for $\theta = 60°$ these relative differences are ~ 20%, ~ 15% and ~ 10%, for Be, Al and Pb, respectively, while for $\theta = 90°$ the respective relative differences are ~ 30%, ~ 25% and ~ 10%. These values are practically the same for $C = 0.2$ and $C = 0.1$.

The agreement between Monte Carlo results and experimental data is even better for the mean energy of the detected photons, as shown in Fig. 8f–j. It should be noted that, unlike the photon yields, these mean energies are not given quantitatively in Faddegon et al. (1990, 1991). Only in Faddegon et al. (1991), the values for the 15 MeV electron beam are shown in a semi-logarithmic plot. The experimental values indicated in Fig. 8f–j have been calculated from the experimental fluences by using the same integration procedure as in the evaluation of the Monte Carlo average photon energies. We have verified that this procedure to evaluate the corresponding integrals produces the same results as those quoted in Faddegon et al. (1991) in the case of the photon yields.

For these mean photon energies, the relative differences between experimental and calculated values are smaller than 5% in all cases analyzed except for Be, the 15 MeV electron beam and the photon detection angles of 60° and 90°. In these two cases the Monte Carlo results clearly underestimate the empirical mean energy (see Fig. 8f) and the relative differences reach −31% for 60° and −28% for 90°. It is worth pointing out that for these mean photon energies the dependency with C is not as pronounced as for the other quantities studied here and there are several cases in which the value obtained for $C = 0.2$ is closer to the experiment than the mean energy calculated with $C = 0.001$.

4. Conclusions

The generation of bremsstrahlung photons by impact of electron beams with energies between 10 and 30 MeV on thick Be, Al and Pb targets has been analyzed by means of the class-II Monte Carlo code system PENELOPE. The role played by the tracking parameters C_1 and C_2 has been investigated by assuming for these parameters the values $C = C_1 = C_2 = 0.2$ (the maximum value allowed by the code), 0.1, 0.01, and 0.001. These parameters determine the cutoff scattering angle, which separates hard elastic collisions (simulated detailedly) from small-angle soft collisions (which are simulated in a condensed way).

Simulated photon yields and mean energies of the detected photons are in fairly good agreement with experimental data for the considered C values. However, there is an expected improvement in that agreement when the C value is decreased. Only in the case of the mean photon energy, no appreciable dependence with the C value has been observed.

The improvement of the intrinsic angular distribution of bremsstrahlung photons, which was introduced in the 2018 version of the PENELOPE code, has been shown to lead to a better description of experimental spectra in the case of lead targets.

To summarize, the present results confirm the reliability of the bremsstrahlung production model implemented in the version 2018 of PENELOPE. Regarding bremsstrahlung fluences, simulations with $C = 0.01$ produce results that agree equally well with experimental data than more detailed simulations performed with $C = 0.001$. The use of the latter increases the simulation time by a factor of about 6.5 without any appreciable gain in accuracy.

CRediT authorship contribution statement

P.A. García-Higueras: Concept, Design, Analysis, Writing, or revision of the manuscript. **S. García-Pareja:** Concept, Design, Analysis, Writing, or revision of the manuscript. **F. Salvat:** Concept, Design, Analysis, Writing, or revision of the manuscript. **A.M. Lallena:** Concept, Design, Analysis, Writing, or revision of the manuscript.

Declaration of competing interest

The authors declare that they have no known competing financial interests or personal relationships that could have appeared to influence the work reported in this paper.

Data availability

Data will be made available on request.

Acknowledgments

The authors thank B. Faddegon for providing them with the whole set of experimental data. This work has been partially supported by the Spanish Ministerio de Ciencia *y* Competitividad (PID2019-104888GB-I00), the European Regional Development Fund (ERDF) and the Junta de Andalucía, Spain (FQM387, P18-RT-3237). Funding for open access charge by Universidad de Granada / CBUA is acknowledged

References

Brualla, L., Rodriguez, M., Lallena, A.M., 2017. Monte Carlo systems used for treatment planning and dose verification. Strahlenther. Onkol. 193, 243–259.

Dance, W.E., Rester, D.H., Farmer, B.J., Johnson, J.H., 1968. Bremsstrahlung produced in thick aluminium and iron targets by 0.5 to 2.8 MeV electrons. J. Appl. Phys. 39, 2881–2889.

Faddegon, B.A., Asai, M., Perl, J., Ross, C., Sempau, J., Salvat, F., 2008. Benchmarking of Monte Carlo simulation of bremsstrahlung from thick targets at radiotherapy energies. Med. Phys. 35, 4308–4317.

Faddegon, B.A., Ross, C.K., Rogers, D.W.O., 1990. Forward-directed bremsstrahlung of 10-30 MeV electrons incident on thick targets of Al and Pb. Med. Phys. 17, 773–785.

Faddegon, B.A., Ross, C.K., Rogers, D.W.O., 1991. Angular distributions of bremsstrahlung from 15 MeV electrons incident on thick targets of Be, Al and Pb. Med. Phys. 18, 727–739.

Lanzl, L.H., Hanson, A.O., 1951. Z dependence and angular distribution of bremsstrahlung from 17-Mev electrons. Phys. Rev. 83, 959–974.

Llovet, X., Salvat, F., 2018. Influence of simulation parameters on the speed and accuracy of Monte Carlo calculations using PENEPMA. IOP Conf. Ser.: Mater. Sci. Eng. 304, 012009.

Nakamura, T., Hirayama, H., 1976. Spectra of bremsstrahlung produced in very thick lead targets by 15-20-, and 25-mev electrons. Nucl. Sci. Eng. 59, 237–245.

Pandola, L., Andenna, C., Caccia, B., 2015. Validation of the GEANT4 simulation of bremsstrahlung from thick targets below 3 MeV. Nucl. Instr. Methods Phys. Res. B 350, 41–48.

Rester, D.H., Dance, W.E., Derrickson, J.H., 1970. Thick target bremsstrahlung produced by electron bombardment of targets of Be, Sn and Au in the energy range 0.2-2.8 MeV. J. Appl. Phys. 41, 2682–2692.

Rodriguez, M., Sempau, J., Brualla, L., 2015. Study of the electron transport parameters used in PENELOPE for the Monte Carlo simulation of linac targets. Med. Phys. 42, 2877–2881.

Salvat, F., 2020. PENELOPE-2018: A code system for Monte Carlo simulation of electron and photon transport, NEA/MBDAV/R(2019)1. OECD Nuclear Energy Agency, Boulogne-Billancourt, http://dx.doi.org/10.1787/32da5043-en.

Salvat, F., Fernández-Varea, J.M., Sempau, J., Llovet, X., 2006. Monte Carlo simulation of bremsstrahlung emission by electrons. Radiat. Phys. Chem. 75, 1201–1219.

Sempau, J., Fernández-Varea, J.M., Acosta, E., Salvat, F., 2003. Experimental benchmarks of the Monte Carlo code PENELOPE. Nucl. Instrum. Methods Phys. Res. B 207, 107–123.